1-1-2012

Impact of mechanical bending on the electrochemical performance of bendable lithium batteries with paper-like free-standing V2O5-polypyrrole cathodes

Lukman Noerochim
University of Wollongong, ln865@uowmail.edu.au

Jia-Zhao Wang
University of Wollongong, jiazhao@uow.edu.au

David Wexler
University of Wollongong, david_wexler@uow.edu.au

Md Mokhlesur Rahman
University Of Wollongong, mrahman@uow.edu.au

Jun Chen
University of Wollongong, junc@uow.edu.au

See next page for additional authors

Journal of Materials Chemistry

Cite this: *J. Mater. Chem.*, 2012, **22**, 11159

www.rsc.org/materials

PAPER

Impact of mechanical bending on the electrochemical performance of bendable lithium batteries with paper-like free-standing V_2O_5–polypyrrole cathodes

Lukman Noerochim,*[ab] Jia-Zhao Wang,[a] David Wexler,[c] Md. Mokhlesur Rahman,[a] Jun Chen[d] and Hua-Kun Liu[a]

Received 9th December 2011, Accepted 20th March 2012
DOI: 10.1039/c2jm16470a

Highly flexible, paper-like, free-standing V_2O_5 and V_2O_5–polypyrrole (PPy) films were prepared *via* the vacuum filtration method. The films are soft, lightweight, and mechanically robust. The electrochemical performance of the free-standing pure V_2O_5 electrode was improved by incorporating conducting polypyrrole. A bendable cell with a novel design was fabricated, consisting of a free-standing V_2O_5–PPy cathode film, gel electrolyte, and a lithium foil anode. The cell was tested under repeated bending conditions for several cycles. The results show that the battery performance of the repeatedly bent cell was similar to that of the conventional cell.

1. Introduction

With recent advances in the technology of various types of flexible portable electronic equipment, such as roll-up displays and medical devices, there has been a strong market demand for small, thin, lightweight, and bendable batteries to power them. Furthermore, wearable electronics, such as wearable displays, embedded health monitoring devices, and wearable military devices also require lightweight and wearable batteries.[1–4] However, conventional lithium batteries typically consist of a positive electrode and a negative electrode spaced by a separator, which is soaked with an electrolyte solution. Each electrode is formed from a metal substrate that is coated with a mixture of an active material, an electrical conductor, and a binder. This kind of electrode is not suitable for flexible or bendable batteries, because a metal substrate is used to hold the active materials. The active material layers will crack or get peeled off the substrate when they are bent frequently. To avoid these drawbacks, mechanically flexible, soft, and free-standing electrode materials are required.[5–10] There are a number of studies on preparing flexible electrodes for lithium ion battery application. Varta microbattery has developed a new generation of thin polymer batteries, PoLiFlex™, using a polymer electrolyte based on a poly(vinylidene fluoride) (PVDF)-copolymer binder matrix.[11] Using this technique, Dennler and co-workers have developed a thin (<1 mm), lightweight (<10 g), and flexible photovoltaic (PV) solar battery module.[12] Carbon-based "bucky" paper also has been studied for preparation of flexible anode materials.[5,10,13] Graphene, carbon nanotubes (CNTs), and their composites have all been proposed and investigated for use as anode materials, but the challenge has remained to find a suitable substrate-free cathode material for lithium ion batteries. Unlike carbon based anodes, conventional cathode materials (*e.g.*, $LiFePO_4$ and $LiCoO_2$) are brittle ceramics that are difficult to form into flexible free-standing structures. Hence, a flexible and free-standing cathode material with excellent electrochemical performance has remained to be discovered.

Recently, two research groups at the University of Wollongong (Australia) and Tsinghua University (China) have reported flexible free-standing VO_2(B) and V_2O_5 nanowire films that were tested as cathode materials for lithium batteries.[9,14] The free-standing electrode materials showed acceptable performance; however, the free-standing materials were tested using coin type cells under normal conditions without any bending. As the free-standing materials are designed for bendable or wearable batteries, it is important that the materials be tested under bending conditions. Therefore, in this study, we designed a soft bendable cell which consisted of a free-standing V_2O_5–polypyrrole (PPy) cathode, a lithium foil anode, and gel polymer electrolyte.

The V_2O_5–PPy composite was synthesized by coating PPy on V_2O_5 nanowires. Polypyrroles have been extensively studied as cathode materials for rechargeable batteries because of their superior electroactivity, good electrical conductivity, and chemical stability.[15–17] PPy has also been used as an additive in electrode materials for battery application to improve the conductivity and to reduce the dissolution of active materials into the electrolyte.[18–21] Based on our previous experience with PPy, we have designed and prepared free-standing V_2O_5–PPy cathode materials based on the following ideas:

[a]*Institute for Superconducting and Electronic Materials, ARC Centre of Excellence for Electromaterials Science, University of Wollongong, NSW 2500, Australia. E-mail: ln865@uow.edu.au; Fax: +61 2 4221 5731; Tel: +61 2 42981494*
[b]*Department of Materials and Metallurgy, Sepuluh Nopember Institute of Technology, Surabaya 60111, Indonesia*
[c]*School of Mechanical, Materials and Mechatronic Engineering, University of Wollongong, NSW 2522, Australia*
[d]*Intelligent Polymer Research Institute, University of Wollongong, NSW 2500, Australia*

(i) Conductive PPy coating on the surface of V_2O_5 nanowires can improve the conductivity of the free-standing electrode. At the same time, PPy can also act as a binder, increasing the contact between the wires[22] and improving the mechanical property of wires.

(ii) The conducting polypyrrole serves not only as a conducting agent to improve the conductivity of free-standing electrode materials, but also as an electrochemically active material to contribute to the capacity. Therefore, using PPy as an additive is better than using some other inert additives, such as CNTs.

(iii) PPy nanoparticles coated onto the surface of V_2O_5 powder may absorb V_2O_5 due to their porous surface morphology and reduce the dissolution of the V_2O_5 into the electrolyte. Consequently, the V_2O_5 utilization and cyclic durability were improved.[23,24]

In practical utility, the bendable and flexible lithium batteries have to maintain both their electrochemical and mechanical performances during daily operation. In the present work, we report the influence of mechanical bending on the electrochemical behavior of bendable lithium batteries consisting of a free-standing V_2O_5–PPy cathode film, gel electrolyte, and a lithium foil anode. The electrochemical performances of the novel bendable cells were tested under repeated bending. Our data indicated that novel bendable cells can be bent to small radii of curvature and still function well.

2. Experimental procedures

2.1 Syntheses of V_2O_5 nanowires and V_2O_5–PPy composite

The hydrothermal method[25,26] was adopted and modified in this work to control the length of nanowires for the preparation of free-standing V_2O_5 films. 0.360 g V_2O_5 powder (98%, Reidel De Haën) was dissolved in 30 ml deionized water and 5 ml 30% H_2O_2 (Sigma Aldrich), and mixed under vigorous magnetic stirring at room temperature until a transparent orange solution was obtained. The resultant solution was then transferred to a 125 ml autoclave and kept in an oven at 200 °C for 24 hours. After naturally cooling to room temperature, the product was washed several times with distilled water.

The V_2O_5–PPy composite was prepared by adding 0.05 M tetrabutylammonium hexafluorophosphate and 0.06 M distilled pyrrole monomer into the solution containing 2 mg ml^{-1} V_2O_5 nanowires. The mixture was stirred until the gradual change of colour from light black to deep black indicated the formation of PPy. The reaction mixture was then kept under the same conditions for 24 h. The synthesized samples were centrifuged and rinsed several times with distilled water and ethanol.

2.2 Preparation of free-standing V_2O_5 and V_2O_5–PPy films

To make a uniform film, a modified vacuum filtration technique was adopted,[27] where a 300 ml filter funnel (Glasco) was used. In a typical procedure, 20 mg of V_2O_5–PPy material was dispersed into 1 wt% Triton X-100 surfactant (Sigma-Aldrich) in 50 ml of distilled water. The suspension was then ultrasonically agitated using a probe sonicator for 1 minute. The as-prepared suspension was poured into the funnel and filtered through a porous polyvinylidene fluoride (PVDF) membrane (Millipore, 0.22 μm pore size, 47 mm in diameter) by applying positive pressure from a vacuum pump. The solvent passed through the pores of the membrane, but the V_2O_5–PPy material was trapped on the membrane surface, forming a mat. The resultant mat with its PVDF membrane was then washed twice using distilled water, followed by ethanol to remove any remaining solvent. The mat with the PVDF membrane still attached was dried in an oven for 2 hours and then peeled off the membrane.

2.3 Preparation of gel polymer electrolyte and fabrication of bendable cell

Poly(vinylidenefluoride-*co*-hexafluorpropylene) P(VDF-HFP) was used as received from Sigma-Aldrich. *N*-Methylpyrrolidinone (NMP) and nanoscale Al_2O_3 powders each with an average particle size of 30 nm were obtained from Sigma-Aldrich. 1 M $LiPF_6$ solution in ethylene carbonate (EC)–dimethyl carbonate (DMC) was purchased from Merck Co. and used without any treatment. A porous film was prepared by the liquid–liquid extraction process.[28] A certain amount of P(VDF-HFP) was dissolved in NMP at 50 °C. Then, the nanoscale Al_2O_3 particles were added to the viscous solution and agitated with an ultrasonic stirrer. The resulting slurry was cast onto the surface of the free-standing V_2O_5–PPy electrode and dried under vacuum at 80 °C for 8 h. After evaporation of the NMP, the electrode with gel electrolyte precursor was soaked in a 1 mol l^{-1} solution of $LiPF_6$/EC–DMC (volume 1 : 1) for 1 h. The surface of the electrode with gel electrolyte was wiped clean with filter paper, and then the electrode with gel electrolyte was fabricated into flexible bendable cells with lithium foil as the counter-electrode. Flexible and soft aluminium laminated pack materials (provided by DLG Battery Co., Ltd, Shanghai, P.R. China) were used to assemble the bendable cells. Fig. 1 contains a schematic diagram of a typical flexible and bendable cell for bending-state electrochemical testing.

2.4 Structure, morphology analysis, and mechanical property testing

X-ray diffraction (XRD) data were collected on a GBC MMA generator and diffractometer with Cu Kα radiation. For infrared (IR) spectroscopy, the samples were mixed with KBr powder, placed in a sample holder, and measured using a Shimadazu IRPrestige-21 Fourier transform IR (FT-IR) spectrometer. KBr was used as the background file. All spectra were measured from

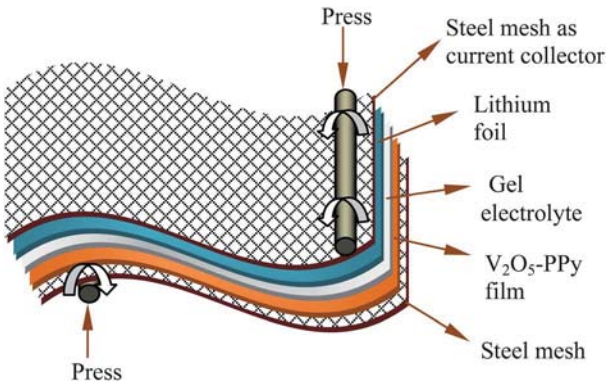

Fig. 1 Schematic diagram of a flexible cell for bending-state electrochemical testing.

2000 to 400 cm^{-1}, and the number of scans was typically 10, with a resolution of 2 cm^{-1}. The amount of PPy in the sample was estimated using a thermogravimetric analysis/differential scanning calorimetry (TGA/DSC) 1 Stare System. The morphologies of the films were investigated by field emission scanning electron microscopy (FESEM, JEOL JSM-7500FA) and transmission electron microscopy (JEOL 2011, 200 kV). The mechanical properties of the free-standing films were investigated with a Shimadzu EZ-S Universal Testing Machine. Tensile tests were conducted under a fixed stretching speed of 1 mm min^{-1} for all specimens. The specimens were 5 mm in width and 30 mm in length.

2.5 Electrochemical measurements

The free-standing electrodes were tested in coin-type cells to confirm the initial electrochemical performance. CR 2032 coin-type cells were assembled in an Ar-filled glove box (Mbraun, Unilab, Germany) by stacking a porous polypropylene separator containing liquid electrolyte between the V_2O_5–PPy free-standing film electrode and the lithium foil counter-electrode. The electrolyte used was 1 M $LiPF_6$ in a 50 : 50 (v/v) mixture of ethylene carbonate (EC) and dimethyl carbonate (DMC), provided by MERCK KgaA, Germany. The bendable cells were also assembled in the glove box with free-standing V_2O_5–PPy cathode, lithium foil anode, and gel electrolyte. Charge–discharge tests were carried out with a battery testing device (Land battery tester) interfaced to a computer with software. The system is capable of switching between charge and discharge automatically according to the pre-set cut-off potentials. The cells were cycled between 1.5 and 4.0 V with a constant current of 40 mA g^{-1}. The change in conductivity after each repeated bending was examined by electrochemical impedance spectroscopy (EIS) measurements using a sine wave of 10 mV amplitude over a frequency range of 100 kHz to 0.01 Hz.

3. Results and discussion

Fig. 2(a) shows the X-ray diffraction (XRD) patterns of the V_2O_5 film, the V_2O_5–PPy film, and commercial V_2O_5. All the diffraction peaks can be indexed as orthorhombic V_2O_5 phase with the lattice parameters $a = 11.54$ Å, $b = 3.571$ Å, and $c = 4.383$ Å, in good agreement with the literature (JCPDS card no. 89-0612). No characteristic peaks of any impurities were detected in these patterns. Compared to the commercial V_2O_5, the relatively strong intensities of the (200) and (400) diffraction peaks of the V_2O_5 nanowires indicate that there is a preferred distribution of planes parallel to the *a*-direction. The formation of orthorhombic V_2O_5 single crystalline nanowires is probably related to the layered structure of $V_2O_5 \cdot nH_2O$.[29] V_2O_5 dissolves in distilled water in the presence of H_2O_2 to form an orange solution of diperoxo anions, $VO(O_2)_2(OH_2)^-$. The H_2O_2 in excess and peroxo groups are slowly oxidized, giving oxygen gas. Monoperoxo and dimer species are then progressively formed as peroxo groups are decomposed. An aqueous solution of VO_2^+ and $H_2V_{10}O_{28}^{4-}$ is finally obtained.[30,31] At the early stage of hydrothermal treatment of the aqueous solution of VO_2^+ and $H_2V_{10}O_{28}^{4-}$, $V_2O_5 \cdot nH_2O$ fibres with large diameters are obtained due to the condensation of vanadic acid *via* a homogeneous nucleation and solution growth process.

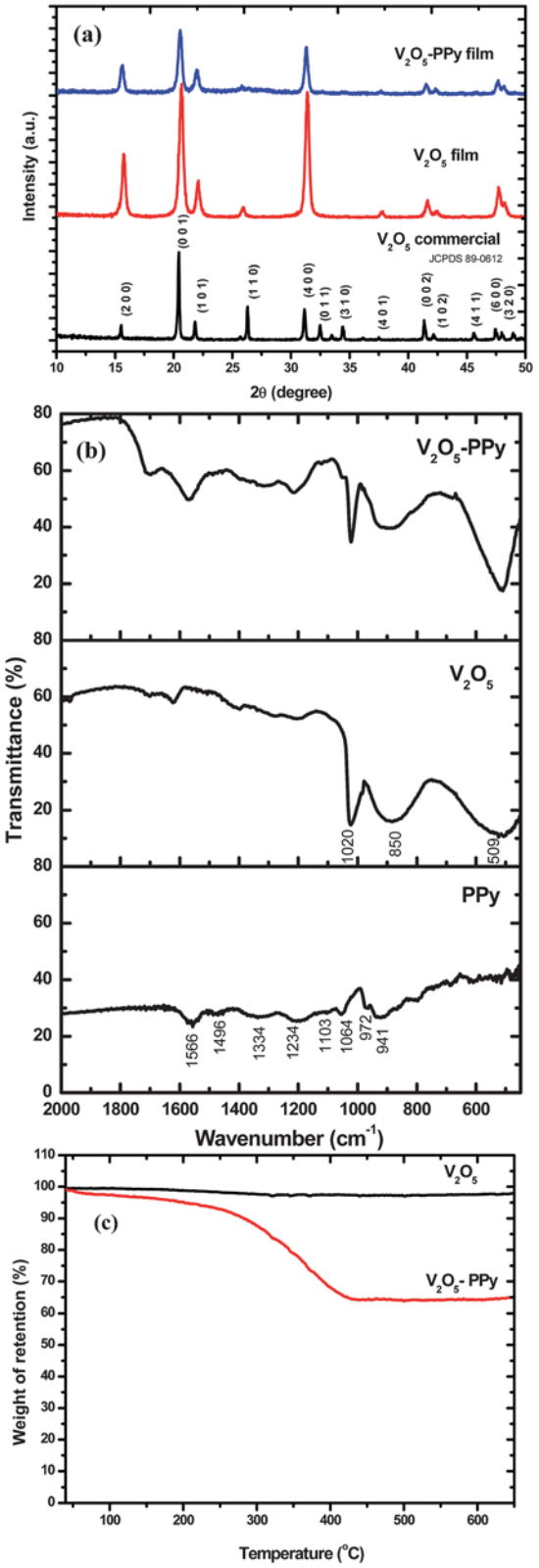

Fig. 2 (a) XRD patterns of V_2O_5 film, V_2O_5–PPy film, and commercial V_2O_5; (b) FTIR transmission spectra of V_2O_5–PPy, V_2O_5 and PPy; and (c) TGA curve of V_2O_5 and V_2O_5–PPy film.

As the reaction proceeds, crystalline V_2O_5 is formed *via* dehydration and recrystallization of $V_2O_5 \cdot nH_2O$, and the fibrillar precipitates can be cleaved along the planes due to their large interplanar spacing, so V_2O_5 single-crystalline nanowires are formed.

The FT-IR spectra of pure PPy and V_2O_5–PPy films are shown in Fig. 2(b). It is clear that the two spectra are similar to each other, indicating that the main polymer chains of the V_2O_5–PPy hybrid are similar to those of PPy. The features at 1566 and 1496 cm^{-1} were attributed to the antisymmetric and symmetric pyrrole ring vibrations, respectively. The peaks at 1334 and 1064 cm^{-1} were ascribed to the in-plane C–H stretching vibration and in-plane N–H deformation, respectively. The bands at 1234 and 972 cm^{-1} reflected the C–N stretching vibration and the =C–H out-of-plane vibration, which implied the doping state of PPy.[32,33] The other peaks, centred at 1103 and 941 cm^{-1}, were assigned to the hydroxyl group peaks. For V_2O_5–PPy hybrid, besides the above characteristic peaks belonging to PPy, the vibration modes of V_2O_5 were detected. The peaks at 1020, 850, and 509 cm^{-1} were attributed to the terminal oxygen symmetric stretching mode (ν_s) of V=O and the bridge oxygen asymmetric and symmetric stretching modes (ν_{as} and ν_s) of V–O–V, respectively.[33–35] In addition, some minor spectroscopic differences and displacements were observed, which showed that there was physical interaction between polypyrrole and V_2O_5 in the hybrid material.

For quantifying the amount of PPy in the V_2O_5–PPy materials, TGA was carried out in air (Fig. 2(c)). The samples were heated from 30 to 650 °C at a rate of 10 °C min^{-1}. As can be seen from Fig. 2(c), V_2O_5–PPy powders started to lose weight slowly in air with increasing temperature, and maximum weight loss was found to take place around 80 to 400 °C, while the bare V_2O_5 powders remained stable over the entire temperature range. As the V_2O_5 powders remained stable over this temperature range, any weight change is believed to correspond to the oxidation of PPy. Therefore, the change in weight before and after the oxidation of PPy directly translates into the amount of PPy in the V_2O_5–PPy film. By the use of this method, it was estimated that the amount of PPy in the V_2O_5–PPy film was approximately 35 wt%.

FESEM observations of the V_2O_5 and V_2O_5–PPy films are presented in Fig. 3. The FESEM image of pristine V_2O_5 film (Fig. 3(a)) shows straight nanowires ~80 to 120 nm in diameter and several microns in length, resulting in an aspect ratio of $\sim 10^2$ to 10^3. Some of the V_2O_5 nanowires are isolated or grown-together in the form of bundles, as shown in the inset. On the other hand, the V_2O_5–PPy film (Fig. 3(b)) shows similar morphology to the V_2O_5 film, with the PPy uniformly deposited throughout entire lengths of nanowires with irregular or spherical shapes. The cross-sectional view of the V_2O_5–PPy film (Fig. 3(c)) shows that the V_2O_5–PPy film is composed of very dense web-like nanowires joined together in a well packed layer, with the thickness of the flexible electrode around 10 μm. The pristine V_2O_5 and V_2O_5–PPy free-standing films can be rolled up (Fig. 3(d) and (e)) or bent to any curvature, and then returned to their original shape, while still maintaining their useful properties. Fig. 3(f) shows the stress–strain curves of flexible V_2O_5 and V_2O_5–PPy film electrodes. The V_2O_5–PPy film (black curve) presents a significantly higher modulus than the pure V_2O_5 film (red curve), indicating that the V_2O_5–PPy could sustain much higher stress compared with V_2O_5 without the PPy coating. This suggests that the PPy coating does

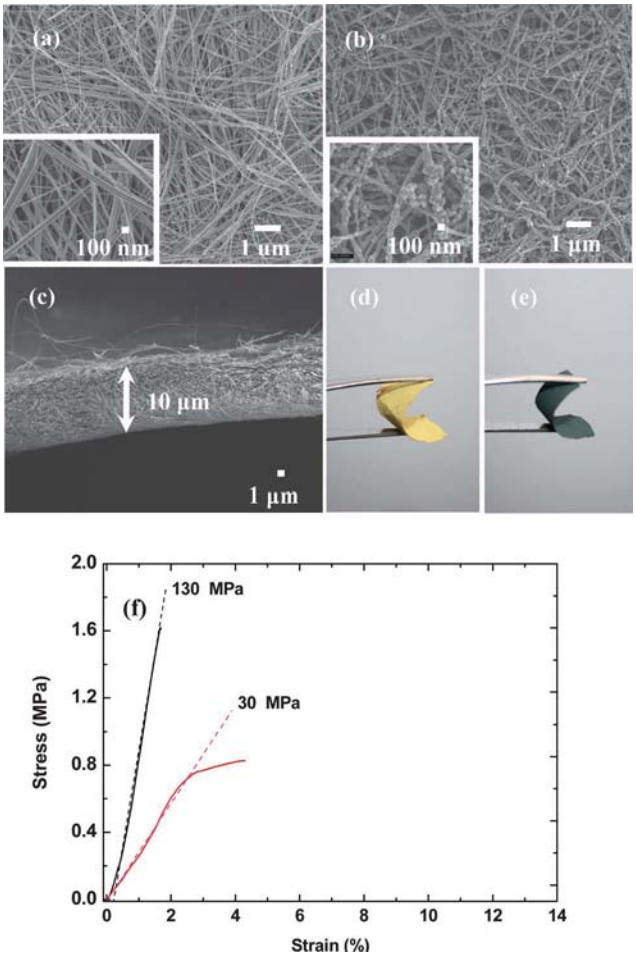

Fig. 3 FESEM images: top view of free-standing V_2O_5 film (a) and V_2O_5–PPy film (b) with inset high magnification images; cross-sectional view at low magnification of free-standing V_2O_5–PPy film (c). Photographs demonstrating the flexibility of the V_2O_5 film (d) and the V_2O_5–PPy film (e). Stress and strain curves of V_2O_5 and V_2O_5–PPy film samples (f).

improve the mechanical strength and greatly enhances the stiffness of the V_2O_5–PPy; however, the toughness was decreased (as the area under the stress–strain curve for pure V_2O_5 is larger than that for V_2O_5–PPy).

Preliminary TEM investigations revealed additional information concerning the structural and morphological evolution of the samples, as shown in Fig. 4. The PPy layer, as revealed in low (Fig. 4(a)) and high (Fig. 4(b)) magnification images, fairly coats entire lengths of nanowires. Based on selected area electron diffraction (not shown) it was also clear that the V_2O_5 nanowires exhibit a well-ordered multilayered structure. High-resolution TEM (HRTEM) imaging of individual nanowires (Fig. 4(b)) revealed lattice fringes, in a good agreement with orthorhombic V_2O_5 (JCPDS card no. 89-0612). The contrast from the indicated (200) V_2O_5 fringes, is confirmed by the occurrence of spots in the associated fast Fourier transform (inset of Fig. 4(b)). The fringe contrast is reduced because of the uniform PPy coating. The HRTEM contrast produced by PPy coating itself (edge of coated nanowire, Fig. 4(b)) is typical of an amorphous hydrocarbon coating.

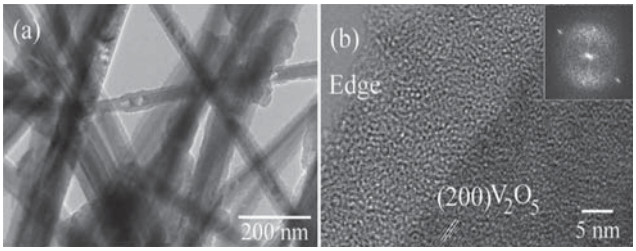

Fig. 4 TEM images: (a) low magnification image of V_2O_5–PPy film, and (b) HRTEM image of the edge of an individual V_2O_5–PPy nanowire with inset fast Fourier transform.

Fig. 5 shows selected cycles of charge–discharge curves for the pristine V_2O_5 film and V_2O_5–PPy film electrodes in the coin cells at a current density of 40 mA g^{-1} between 1.5 and 4.0 V *vs.* Li/Li^+. The pristine V_2O_5 and V_2O_5–PPy film electrodes show three discharge plateaus for initial discharge, indicating a similar reaction mechanism for Li^+ ion intercalation into V_2O_5[36–38] (Fig. 5(a) and (b)). The voltage plateaus appearing above 3.0 V correspond to the structural modifications from V_2O_5 to $Li_xV_2O_5$ for up to one equivalent ($x = 1$) Li^+ insertion. The additional potential plateaus that appear at voltage levels around 2.5 V are attributed to the structural modifications related to Li^+ insertion of greater than one equivalent. Further discharge of the batteries leads to the last plateau at approximately 2.0 V, with an electrochemical insertion of up to three equivalents of Li^+ into the lattice and the ensuing formation of $Li_3V_2O_5$ ($x = 3$ for $Li_xV_2O_5$) during the first discharge process for the extended potential range.[39] The pristine V_2O_5 electrode film (Fig. 5(a)) shows a large initial discharge capacity of 430 mA h g^{-1}, but the first charge capacity is low, only 337 mA h g^{-1}, with a coulombic efficiency of around 78%. The possible reason for such a high discharge capacity may be the larger specific surface area of the V_2O_5 nanowire film electrode. After 100 cycles, the pristine V_2O_5 paper shows a decreased discharge capacity of around 33 mA h g^{-1} and an average coulombic efficiency of 96%. Fig. 5(b) shows typical charge and discharge curves of the V_2O_5–PPy film electrode. The V_2O_5–PPy electrode paper shows an initial discharge capacity of 313 mA h g^{-1}, with a coulombic efficiency of 90%, which is slightly higher than that of the pristine V_2O_5 paper. The 100th discharge capacity of the V_2O_5–PPy film electrode is 188 mA h g^{-1}, which is much better than that of the pristine V_2O_5 film. It can be observed that the V_2O_5–PPy film electrode has a higher specific capacity than the V_2O_5 film electrode throughout the whole initial discharge curve. The conductive PPy polymer in the V_2O_5–PPy film electrode evidently has aided Li^+ intercalation into the $Li_xV_2O_5$ lattice of the V_2O_5–PPy electrode, by improving

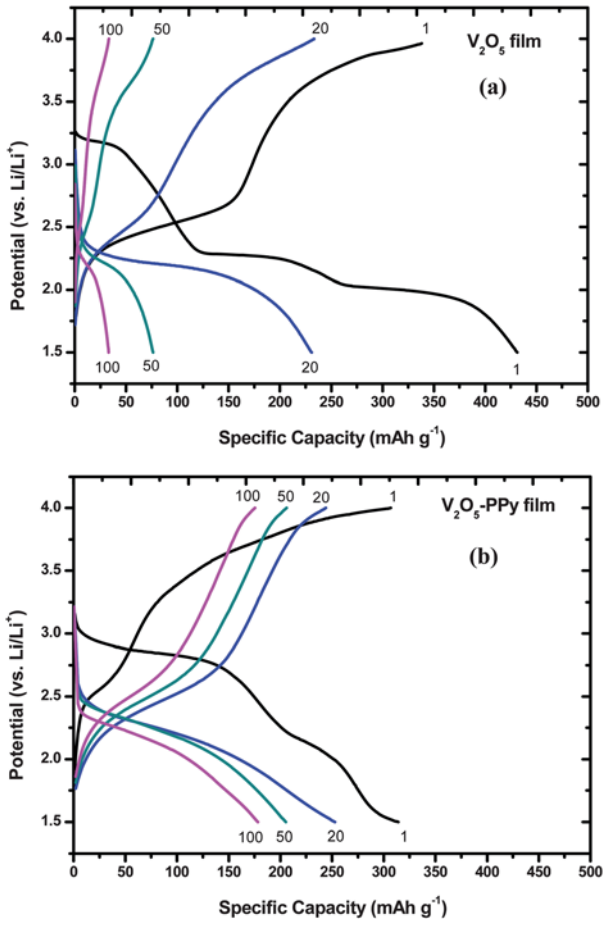

Fig. 5 Typical charge–discharge voltage profiles for selected cycles of (a) V_2O_5 and (b) V_2O_5–PPy film electrodes at a constant current density of 40 mA g^{-1}.

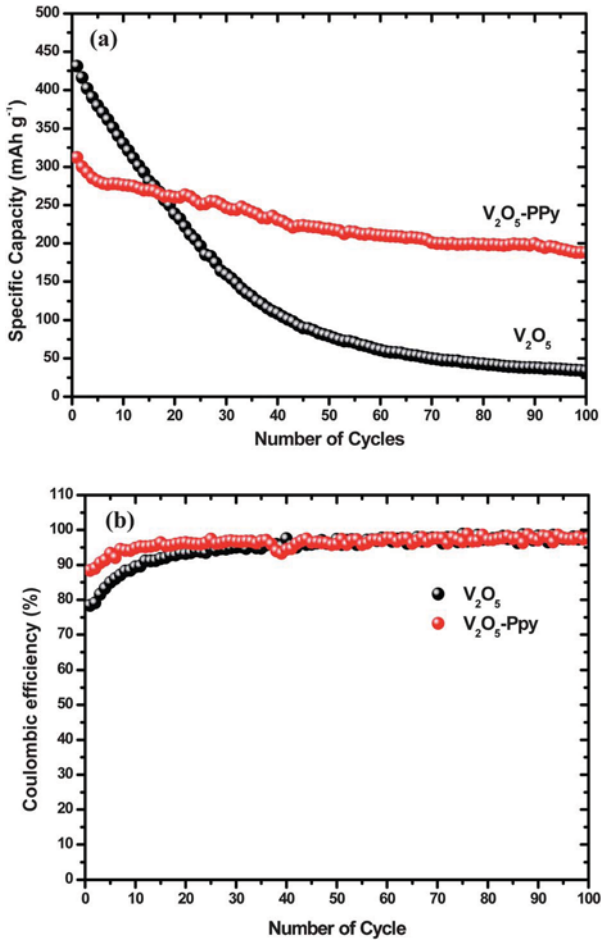

Fig. 6 (a) Cycling stability and (b) Coulombic efficiency of the V_2O_5 and V_2O_5–PPy electrodes at a constant current density of 40 mA g^{-1}.

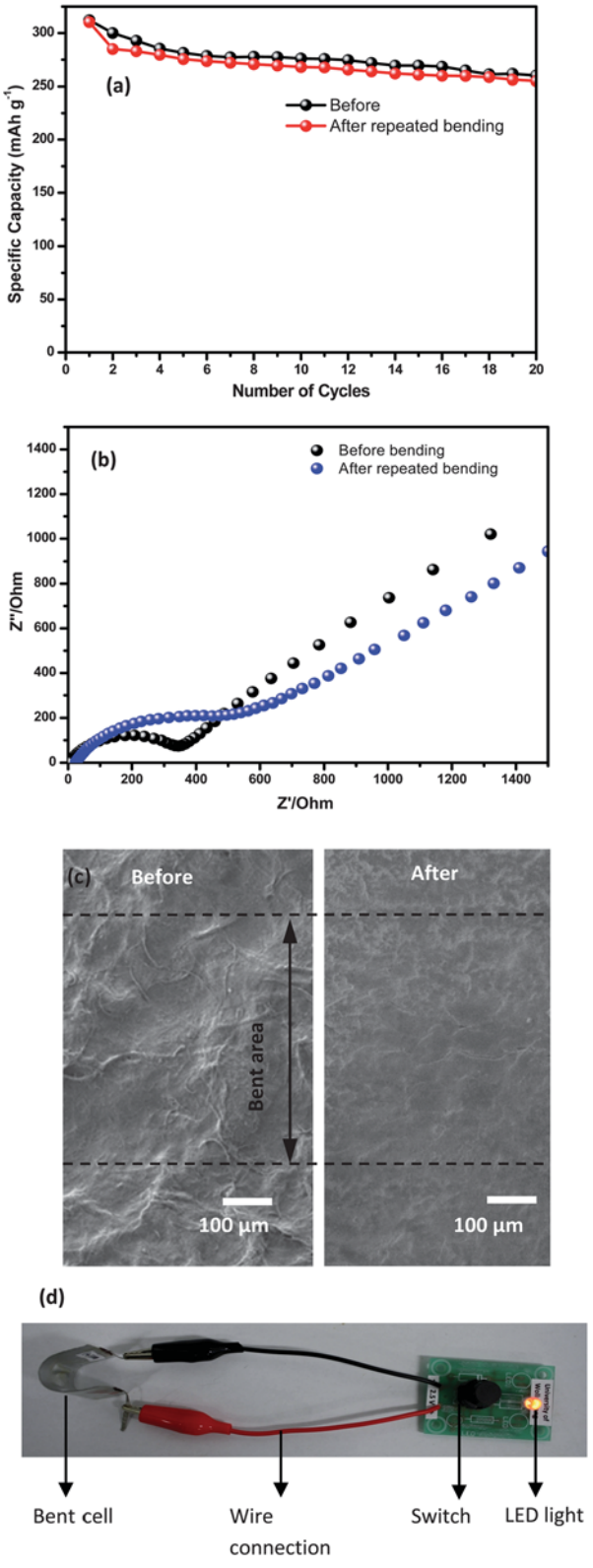

Fig. 7 (a) The cycling stability V_2O_5–PPy film electrode under repeated inward bending at a constant current density of 40 mA g^{-1}; (b) Nyquist plots of cells containing the V_2O_5–PPy film electrodes before and after bending; (c) FESEM images of sample before and after repeated-bending tests; and (d) photograph of cell bent inwards at 180° that was used to power a red LED. The LED glowed even when the battery device was bent, and the demonstration could be repeated over several cycles.

both the accessibility of the Li^+ ions and the electrical conductivity.[39] Conductive polymers in the V_2O_5–PPy film electrode can connect isolated V_2O_5 nanowires and give rise to valid conductive networks in the electrodes.

The cycling stabilities of the pristine V_2O_5 and the V_2O_5–PPy film electrodes are shown in Fig. 6. The discharge capacity of the V_2O_5 and V_2O_5–PPy film electrodes at the 100th cycle are 33 and 187 mA h g^{-1}, respectively. The cell containing the V_2O_5–PPy film cathode exhibits a higher capacity than the battery containing the pristine V_2O_5 film cathode. The results show that electrically conductive and electrochemically active organic polymer (PPy) enhances the specific capacity by connecting isolated V_2O_5 nanowires, thus creating valid conductive networks for lithium ions and/or counter-anions of the electrolyte for the electrode. This enables increased activation of isolated V_2O_5 nanowires and allows them to be employed for lithium intercalation–deintercalation in the V_2O_5–PPy film electrode during the battery cycling.

In order to explore the influence of the mechanical bending of flexible V_2O_5–PPy film electrodes on their electrochemical performance, flexible cells were repeatedly bent inward to an angle of 180°. A flexible cell was bent for up to a total of 10 times, and its capacity and cycling performance were tested for several cycles. Fig. 7(a) shows the initial specific discharge capacity (300 mA h g^{-1}) of a cell. After the bending, the capacity is similar to that of the unbending coin cell (313 mA h g^{-1}). These results demonstrated that the electrochemical behaviour of the free-standing electrodes was slightly influenced by mechanical stress. Further investigation was carried out to explore the influence of repeated bending of flexible V_2O_5–PPy film electrodes on their conductivity by electrochemical impedance spectroscopy (EIS) measurements.

EIS tests were carried out before and after the repeated-bending test. Their change in conductivity after repeated bending was examined by EIS measurement using a sine wave of 10 mV amplitude over a frequency range of 100 kHz to 0.01 Hz (Fig. 7(b)). The results show that the application of bending stress relatively decreased the conductivity of the electrode. After the bending, the conductivity of the cell was 1.74×10^{-4} S m^{-1}, which is slightly lower than that of the unbent cell (2.73×10^{-4} S m^{-1}). SEM images of the free-standing V_2O_5–PPy before and after the bending are shown in Fig. 7(c). No cracks were detected in the electrode around the bent area after the bending test. This suggests that the electrode is resistant to repeated bending. A marginal decrease of the conductivity of the bent cell could be due to the loose contact between Li foil as anode and V_2O_5–PPy film after repeated bending. To show the reliability of the flexible cell after the bending test, the cell is tested to light up a red light-emitting diode (LED) as shown in Fig. 7(d).

4. Conclusions

In this work, a free-standing flexible V_2O_5–PPy film electrode has been prepared by the vacuum filtration method. Electrochemical measurements showed that the V_2O_5–PPy film delivered a significantly higher reversible capacity than the pristine V_2O_5 film and an excellent cycling stability (187 mA h g^{-1} at a current density of 40 mA g^{-1} after 100 cycles), which is higher than that of the pristine film. The hybrid material, consisting of a layer-structured metal oxide and a conducting polymer, promotes

a synergistic interaction between the inorganic and organic components. The V_2O_5–PPy film electrodes have higher specific capacities than the V_2O_5 electrode in Li batteries owing to the improved electronic conductivity and the enhanced lithium-ion accessibility in the cathode. The conductive polymers in the V_2O_5–PPy film efficiently connect isolated V_2O_5 nanowires, resulting in the formation of conductive networks in the electrode. Bending the V_2O_5–PPy film electrodes to small radii of curvature has only a slight effect on the electrochemical behaviour in the bending test. The details of bending-state electrochemical testing of the free-standing electrode can provide useful information for further development of flexible and bendable batteries.

Acknowledgements

Financial support provided by the Australian Research Council through the ARC Centre of Excellence for Electromaterials Science and Discovery Project (DP0987805) are gratefully acknowledged. Many thanks also go to Dr T. Silver for critical reading of the manuscript.

Notes and references

1 H. Nishide and K. Oyaizu, *Science*, 2008, **319**, 737–738.
2 L. Hu, H. Wu, F. La Mantia, Y. Yang and Y. Cui, *ACS Nano*, 2010, **4**, 5843–5848.
3 V. L. Pushparaj, M. M. Shaijumon, A. Kumar, S. Murugesan, L. Ci, R. Vajtai, R. J. Linhardt, O. Nalamasu and P. M. Ajayan, *Proc. Natl. Acad. Sci. U. S. A.*, 2007, **104**, 13574–13577.
4 K. T. Nam, D.-W. Kim, P. J. Yoo, C.-Y. Chiang, N. Meethong, P. T. Hammond, Y.-M. Chiang and A. M. Belcher, *Science*, 2006, **312**, 885–888.
5 S. H. Ng, J. Wang, Z. P. Guo, J. Chen, G. X. Wang and H. K. Liu, *Electrochim. Acta*, 2005, **51**, 23–28.
6 J. Chen, Y. Liu, A. I. Minett, C. Lynam, J. Wang and G. G. Wallace, *Chem. Mater.*, 2007, **19**, 3595–3597.
7 J.-Z. Wang, C. Zhong, S.-L. Chou and H.-K. Liu, *Electrochem. Commun.*, 2010, **12**, 1467–1470.
8 J.-Z. Wang, S.-L. Chou, J. Chen, S.-Y. Chew, G.-X. Wang, K. Konstantinov, J. Wu, S.-X. Dou and H. K. Liu, *Electrochem. Commun.*, 2008, **10**, 1781–1784.
9 K. H. Seng, J. Liu, Z. P. Guo, Z. X. Chen, D. Jia and H. K. Liu, *Electrochem. Commun.*, 2011, **13**, 383–386.
10 C. Wang, D. Li, C. O. Too and G. G. Wallace, *Chem. Mater.*, 2009, **21**, 2604–2606.
11 D. Ilic, P. Birke, K. Holl, T. Wöhrle, P. Haug and F. Birke-Salam, *J. Power Sources*, 2004, **129**, 34–37.
12 G. Dennler, S. Bereznev, D. Fichou, K. Holl, D. Ilic, R. Koeppe, M. Krebs, A. Labouret, C. Lungenschmied, A. Marchenko, D. Meissner, E. Mellikov, J. Méot, A. Meyer, T. Meyer, H. Neugebauer, A. Öpik, N. S. Sariciftci, S. Taillemite and T. Wöhrle, *Sol. Energy*, 2007, **81**, 947–957.
13 S. Y. Chew, S. H. Ng, J. Wang, P. Novák, F. Krumeich, S. L. Chou, J. Chen and H. K. Liu, *Carbon*, 2009, **47**, 2976–2983.
14 J. Huang, X. Wang, J. Liu, X. Sun, L. Wang and X. He, *Int. J. Electrochem. Sci.*, 2011, **6**, 1709–1719.
15 P. Novák, K. Müller, K. S. V. Santhanam and O. Haas, *Chem. Rev.*, 1997, **97**, 207–282.
16 T. F. Otero and I. Cantero, *J. Power Sources*, 1999, **81–82**, 838–841.
17 J.-Z. Wang, S.-L. Chou, H. Liu, G. X. Wang, C. Zhong, S. Yen Chew and H. Kun Liu, *Mater. Lett.*, 2009, **63**, 2352–2354.
18 A. Du Pasquier, F. Orsini, A. S. Gozdz and J. M. Tarascon, *J. Power Sources*, 1999, **81–82**, 607–611.
19 J. Wang, J. Chen, K. Konstantinov, L. Zhao, S. H. Ng, G. X. Wang, Z. P. Guo and H. K. Liu, *Electrochim. Acta*, 2006, **51**, 4634–4638.
20 S. Y. Chew, C. Feng, S. H. Ng, J. Wang, Z. Guo and H. Liu, *J. Electrochem. Soc.*, 2007, **154**, A633–A637.
21 L. Yuan, J. Wang, S. Y. Chew, J. Chen, Z. P. Guo, L. Zhao, K. Konstantinov and H. K. Liu, *J. Power Sources*, 2007, **174**, 1183–1187.
22 S. Y. Chew, Z. P. Guo, J. Z. Wang, J. Chen, P. Munroe, S. H. Ng, L. Zhao and H. K. Liu, *Electrochem. Commun.*, 2007, **9**, 941–946.
23 A. Dobley, K. Ngala, S. Yang, P. Y. Zavalij and M. S. Whittingham, *Chem. Mater.*, 2001, **13**, 4382–4386.
24 S.-L. Chou, J.-Z. Wang, J.-Z. Sun, D. Wexler, M. Forsyth, H.-K. Liu, D. R. MacFarlane and S.-X. Dou, *Chem. Mater.*, 2008, **20**, 7044–7051.
25 T. Zhai, H. Liu, H. Li, X. Fang, M. Liao, L. Li, H. Zhou, Y. Koide, Y. Bando and D. Golberg, *Adv. Mater.*, 2010, **22**, 2547–2552.
26 G. Li, S. Pang, L. Jiang, Z. Guo and Z. Zhang, *J. Phys. Chem. B*, 2006, **110**, 9383–9386.
27 W. A. De Heer, W. S. Bacsa, A. Chatelain, T. Gerfin, R. Humphrey-Baker, L. Forro and D. Ugarte, *Science*, 1995, **268**, 845–847.
28 Z. Li, G. Su, D. Gao, X. Wang and X. Li, *Electrochim. Acta*, 2004, **49**, 4633–4639.
29 V. Petkov, P. N. Trikalitis, E. S. Bozin, S. J. L. Billinge, T. Vogt and M. G. Kanatzidis, *J. Am. Chem. Soc.*, 2002, **124**, 10157–10162.
30 B. Alonso and J. Livage, *J. Solid State Chem.*, 1999, **148**, 16–19.
31 C. J. Fontenot, J. W. Wiench, M. Pruski and G. L. Schrader, *J. Phys. Chem. B*, 2000, **104**, 11622–11631.
32 H. S. Kim, D. H. Park, Y. B. Lee, D.-C. Kim, H.-J. Kim, J. Kim and J. Joo, *Synth. Met.*, 2007, **157**, 910–913.
33 D. W. Murphy, P. A. Christian, F. J. DiSalvo and J. V. Waszczak, *Inorg. Chem.*, 1979, **18**, 2800–2803.
34 A. K. Cuentas-Gallegos and P. Gómez-Romero, *J. Power Sources*, 2006, **161**, 580–586.
35 I. Boyano, M. Bengoechea, I. de Meatza, O. Miguel, I. Cantero, E. Ochoteco, J. Rodríguez, M. Lira-Cantú and P. Gómez-Romero, *J. Power Sources*, 2007, **166**, 471–477.
36 C. Delmas, S. Brèthes and M. Ménétrier, *J. Power Sources*, 1991, **34**, 113–118.
37 C. Delmas, H. Cognac-Auradou, J. M. Cocciantelli, M. Ménétrier and J. P. Doumerc, *Solid State Ionics*, 1994, **69**, 257–264.
38 K. West, B. Zachau-Christiansen, T. Jacobsen and S. Skaarup, *Solid State Ionics*, 1995, **76**, 15–21.
39 Y. Kim, J.-S. Kim, M.-T. Thieu, H.-C. Dinh, I.-H. Yeo, W. I. Cho and S.-I. Mho, *Bull. Korean Chem. Soc.*, 2010, **31**, 3109.